Modelling and analyses of helical milling process

Yanling Tian[1,2], Yunpeng Liu[1], Fujun Wang[1]*, Xiubing Jing[1], Dawei Zhang[1], Xianping Liu[2]

[1]Key Laboratory of Mechanism Theory and Equipment Design of Ministry of Education, Tianjin University, Tianjin 300072, China

[2]School of Engineering, University of Warwick, Coventry CV4 7AL, UK

*Author to whom correspondence should be addressed

Email: wangfujun@tju.edu.cn

Abstract:

A comparison between the geometry of the helical milling specialized tool and conventional end mill was firstly introduced. Furthermore, a mathematical model, in which the cutting area was divided into different cutting zones, was established to simulate the cutting depths and volume of the different cutting edges (three kinds) on specialized tool. Accordingly, a specific ratio between the volume removed by different edges and the total hole volume was derived mathematically and modeled using 3D modeling software SolidWorks. Based on the established models, the cutting depths and cutting volume ratio variation trends under different cutting parameters were analyzed. The results showed that the change rules of cutting depths were different in every cutting zone and influenced greatly by the cutting parameters. In addition, the cutting volume ratio changes with different cutting parameters, but it can only vary in certain range due to the structure of the helical milling specialized tool. The cutting volume ratio obtained from the established model shows a good agreement with the data modeled using SolidWorks, proving that the established model is appropriate. Moreover, the undeformed chip geometry was modeled and observed using SolidWorks. The undeformed chip showed a varying geometry with different cutting parameters and it can be optimized to obtain a good cutting condition during helical milling process.

Keywords: Helical milling; Cutting depth; Cutting volume; Chip morphology

1 Introduction

In modern aircraft manufacturing process, thousands of holes need to be made to meet the complex assembly requirements. As an alternative to conventional drilling, helical milling technique offers many advantages. It possesses a better heat dissipation condition, which can reduce

the thermal damage on both the machined surface and the milling tool, and thus improve hole quality and increase the working life of milling tool [1-4]. An improvement in geometrical accuracy, a reduction in burr formation, and a smaller cutting force are observed when the helical milling method is compared with the drilling method [5-7]. Another advantage of helical milling is that it can make different diameter holes only using one tool, which significantly improves the processing efficiency [8].

Recently, a number of research efforts have been directed towards the helical milling in the aspects of the influences of cutting parameters on cutting force, cutting temperature, tool wear and quality of the machined surface [9-12]. However, the variation of cutting parameters directly affects the cutting depth, cutting volume and undeformed chip morphology, and then the changes of these indexes lead to the variation of cutting force, cutting temperature and so on [13-14]. Therefore, it is necessary to build a mathematical model to describe the relationships between the cutting depth, cutting volume and cutting parameters, and have a fundamental research on the change regulations of undeformed chip geometry under varying cutting parameters.

Brinksmeier et al. [15] described mathematically the cutting depths of periphery and front cutting edges of conventional end mill, the ratio between periphery cutting volume and front cutting volume was also discussed. Based on chip-splitting principle and tool's movement feature, Liu et al. [16] designed a new specialized tool for helical milling with distributed multi-point front cutting edge and modeled the undeformed chip morphology using 3D modeling software, the material removal rates for conventional end mill and helical milling specialized tool were also obtained using 3D modeling software. Denkena et al. [17] modeled the undeformed chip geometry for helical milling in which the axial depth of cut of periphery cutting edges is assumed to increase approximately linearly with the tool rotation angle, and used it to explain the impact of the axial and tangential feed per tooth on the process forces. Li et al. [18] described the cutting depths and undeformed chip geometry of conventional end mill, then proposed a novel dynamic cutting force model for helical milling. Chen et al. [19] presented a new dynamic cutting force model with nominal chip thickness for predicting the stability of interrupted turning, in where the dynamical cutting force was defined by a function of nominal chip thickness and dynamical chip thickness. Liu et al. [20] proposed an analytical model to accurately predict the cutting forces and torque during helical milling operations as a function of helical feed, spindle velocity, axial and radial cutting depth and milling tool geometry.

The cutting depth is essential during the cutting force modelling, and the cutting volume ratio can reflect contribution of different cutting edges during the material removing process. The undeformed chip geometry is useful for the prediction of cutting force and surface quality [21]. However, there are no reports on the theoretical calculation method of cutting depths and cutting volume for helical milling specialized tool. There is also little information available in literature about change rules of undeformed chip geometry of specialized tool under different cutting parameters so far. Therefore, it is necessary to establish the models for the cutting depth and cutting volume of helical milling specialized tool, investigate the effects of the helical course (a_p) and eccentricity (e) on the cutting depths, cutting volume, volume ratio and undeformed chip geometry based on the established models, and obtain the change regulations of the undeformed chip geometry.

2 Helical milling process

In helical milling process, strong interaction will happen between tool and workpiece [22]. Thus, high performance is demanded for the milling tool. The structures of conventional end mill and helical milling specialized tool are shown in Fig. 1. Different from the structure of conventional end mill, the front cutting edge of the helical milling specialized tool is composed of two parts: the part far from tool axis is called outside front cutting edge (outside edge) and the part near tool axis is called inside front cutting edge (inside edge). This special structure makes it participate in a discontinuous cutting and produce discontinued chips.

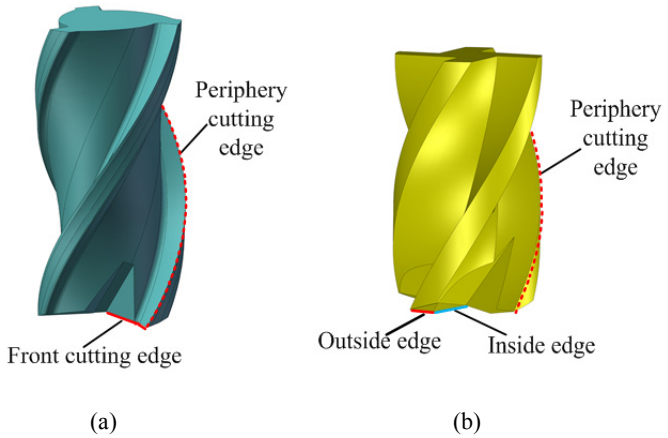

Fig. 1 Structure of two different helical milling tools: **a** conventional end mill **b** helical milling specialized tool

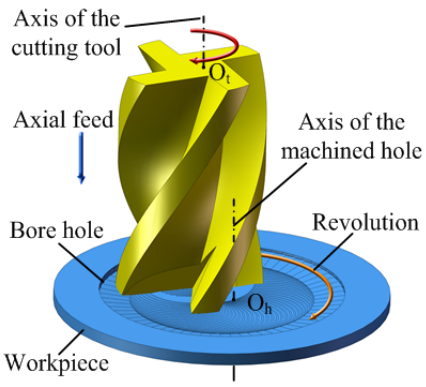

Fig. 2 Kinematics of helical milling

Helical milling is composed of three movements: rotation about the tool axis (spindle rotation), rotation about the axis of the machined hole (revolution), linear motion along with the axis direction of the machined hole (Fig. 2). The circumferential feed and axial feed are provided respectively by revolution and linear motion of the tool. It is convenient to change the machining diameter of hole by varying the eccentricity (e) between the axis of tool and the axis of hole. Different cutting edges produce different types of cutting force. When adopting different cutting parameters, the volume of material removed by periphery cutting edge and front cutting edge will change and lead to the variation of cutting force components in axial and radial direction. Therefore, the material removal rate is also a parameter worthy of further study.

3 Cutting depths of periphery cutting edge, inside edge and outside edge

In helical milling process, all cutting edges are involved directly and cutting states vary with different cutting parameters. In order to observe and analyze the cutting depths, the machined surface is modeled with SolidWorks. Fig. 3 shows the geometrical conditions between the tool and workpiece, there are three cutting zones in helical milling process: the periphery cutting zone, the outside cutting zone, the inside cutting zone.

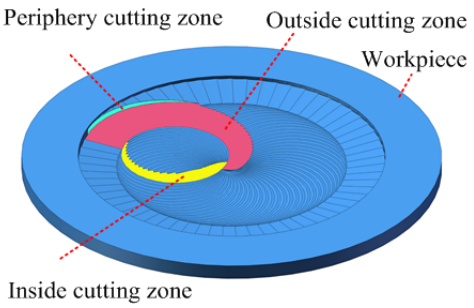

Fig. 3 Three cutting zones between tool and workpiece during helical milling process

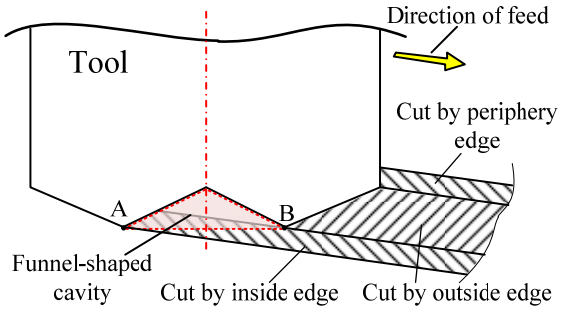

Fig. 4 Schematic drawing of material removal process

Fig. 4 shows the cutting states of periphery cutting edge, inside edge and outside edge. In the cutting process, outside edge will contact with the workpiece and cut off a part of the material first. A funnel-shaped cavity will generate under inside edge when the tool rotates around its axis due to the inclination of the inside edge, the material in the cavity will be removed by inside edge. The material remaining between the two orbital periods that outside and inside edges can't remove will be cut by the periphery cutting edge.

For calculation simplification，a projection plane through the tool axis (Fig. 5(a)) is built and the endpoints of cutting edges on one cutter tooth are revolved around tool axis to the projection plane. Fig. 5(b) shows the graph of cutting edges on projection plane. R_m is the distance from the lowest point C' on the front cutting edge to the tool axis, θ_1 and θ_2 are angles between the projection lines of the cutting edges and the horizontal plane.

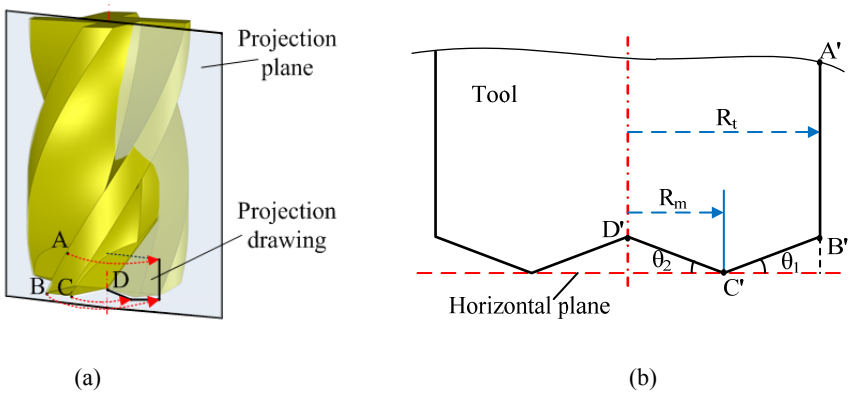

Fig. 5 Projection of the helical milling specialized tool: **a** projection diagram **b** graph of cutting edges on projection plane

In order to further investigate the cutting stages of the cutting edges and determine the periphery cutting depth (h_{1i}), inside cutting depth (h_{2i}) and outside cutting depth (h_{3i}), the variable R_i

(arbitrary inspection radius) is also introduced to help find the relationships between cutting depths (h_{1i}, h_{2i}, h_{3i}) and parameters (R_h, R_t, R_m, a_p, θ_1, e) [15].

For the calculation the following variables are used:

R_h: hole radius R_t: tool radius

a_p: depth setting of the helical course h_{1i}: cutting depth of periphery edge

h_{2i}: cutting depth of inside edge h_{3i}: cutting depth of outside edge

R_i: arbitrary inspection radius e: eccentricity

The value of depth setting of the helical course (a_p) has a significant influence on cutting depths. With the increasing of a_p, the cutting depths of all kinds of cutting edges increase gradually and uncut material under the tool shows different morphologies. To some extent, the morphology of uncut material formed by the tool can reflect the variation trend of the cutting depths. By observing the 3D models formed using SolidWorks, it is noted that there are four types of morphology when the a_p changes from small to large (Fig. 6). In the first type, the helicoid is divided into three regions when the a_p is small enough. In the second type, the helicoid is divided into four regions when the value of a_p exceeds the threshold value a_{p1}. In the third type, the helicoid is divided into three regions when the a_p exceeds the threshold value a_{p2}.In the last type, the helicoid contains only one region when the a_p exceeds the threshold value a_{p3}.

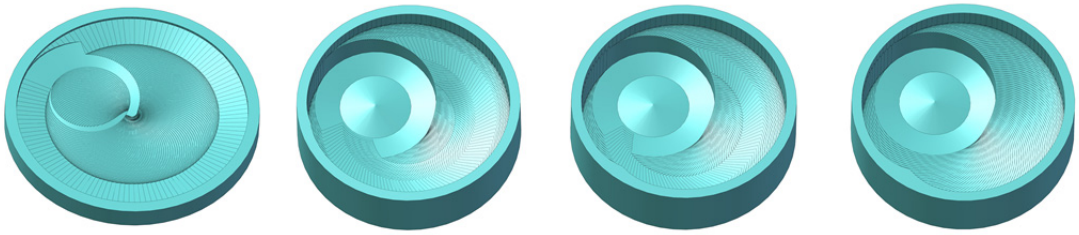

(a) (b) (c) (d)

Fig. 6 Four types of uncut material morphology: **a** the first type **b** the second type **c** the third type **d** the fourth type

Through the observation of the uncut material morphology, the conclusion can be obtained that the cutting depth of the periphery cutting edge can always be reduced to zero within the limits of 0~π. In different regions, the change rules for cutting depths are various. In following sections, the computational method of cutting depths in different kinds of uncut material morphology is discussed.

3.1 Cutting depth of periphery cutting edge

3.1.1 The first type of uncut material morphology (condition 1)

In this condition, the helicoid is divided into three regions shown in Fig. 7(a). It can be seen that the width of the region 1 is very small when comparing with the widths of region 2 and 3. The region 1 is formed by periphery cutting edge; the region 2 is formed by outside cutting edge; the region 3 is formed by inside cutting edge. Fig. 7(b) shows the second type of uncut material morphology. Four regions can be seen in condition 2. When compared with Fig. 7(a), the regions 1, 2, 3 in two conditions are the same, but the region 4 only appears in condition 2. The region 4 is also formed by periphery cutting edge.

In Fig. 8, with the value of a_p increasing, the chip formed by periphery cutting edge may come into being in different regions and there are four possible status: a) only in region 1, b) in region 1 and 2, c) in region 1, 2, 3 but not reach maximum, d) reach maximum.

In regions 1, 2, 3, the calculation methods of periphery cutting depth (h_{1i}) are uniform in condition 1 and 2. Therefore, the derivation of periphery cutting depth (h_{1i}) in condition 1 is not listed here.

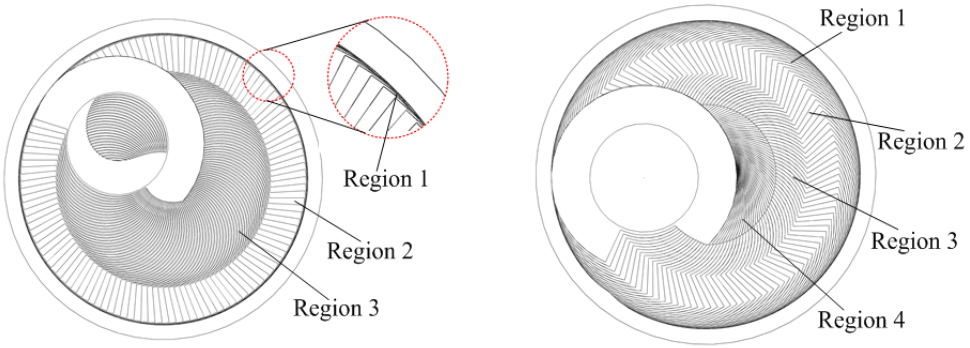

Fig. 7 Regional division of the uncut material: **a** three regions in condition1 **b** four regions in condition 2

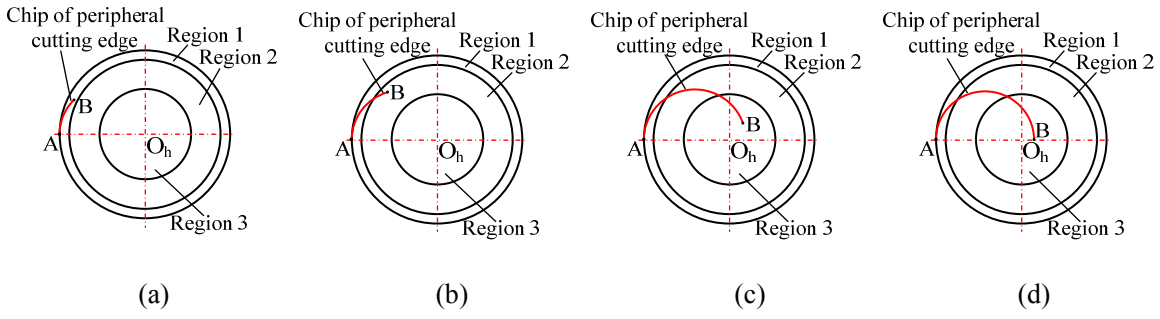

Fig. 8 Periphery cutting chips generated in different regions: **a** region 1 **b** region 1, 2 **c** region 1, 2, 3 **d** reach maximum

3.1.2 The second type of uncut material morphology (condition 2)

In this condition, the helicoid is divided into four regions and the cutting trajectory of periphery cutting edge from point A to E is also divided into four segments (Fig. 9). The change rules of periphery cutting depth (h_{1i}) are different in every region. The variation of cutting depth of periphery cutting edge can be divided into two parts: one part comes from the decrease along the radial direction and another part comes from the decrease along circumferential direction. In order to show the different change rate between the two parts in every region, the variable r is introduced. The radiuses of boundaries between different regions are denoted by R_1, R_2 and R_3.

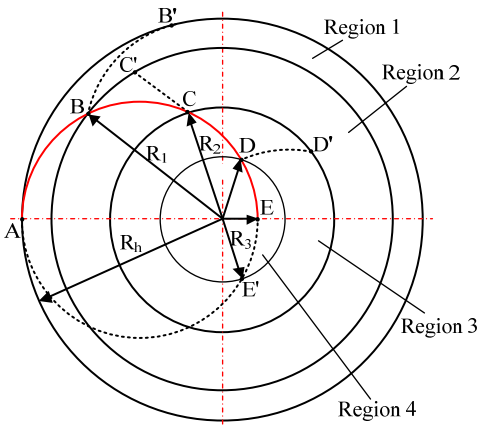

Fig. 9 Four segments of the cutting trajectory of periphery cutting edge in condition 2

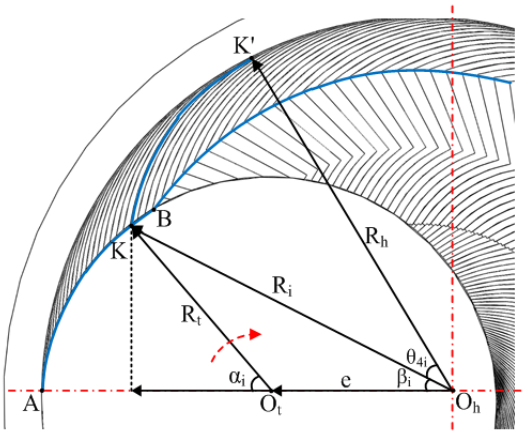

Fig. 10 Graphic for the calculation of h_{1i} in region 1

Region 1: As shown in Fig. 10, the periphery cutting edge cut into the material in point A and moves along the clockwise. When the periphery cutting edge moves to point K, the decrease along

circumference direction can be calculated using angle β_i and the decrease along the radial direction can be replaced by the decrease along circumference direction from K to K' (corresponding to angle θ_{4i}). According to the geometrical relationship in Fig. 10, it is noted that $\theta_{4i}=\beta_i$. Therefore, the decrease of cutting depth along radial direction (h_{1211i}) is equal to the decrease along circumference direction (h_{1212i}) in region 1 and the following equations can be obtained.

$$h_{1211i} = a_p \cdot \frac{\theta_{4i}}{2\pi} \tag{1}$$

$$h_{1212i} = a_p \cdot \frac{\beta_i}{2\pi} \tag{2}$$

Fig. 10 shows the geometrical relationships for angle β_i. According to the law of cosines, the following equation can be derived.

$$\beta_i = \arccos\left(\frac{R_i^2 + e^2 - R_t^2}{2eR_i}\right) \tag{3}$$

Since $\theta_{4i}=\beta_i$, substituting Eq. (3) into Eqs. (1) and (2) gives:

$$h_{1211i} = \frac{a_p}{2\pi}\arccos\left(\frac{R_i^2 + e^2 - R_t^2}{2eR_i}\right) \tag{4}$$

$$h_{1212i} = \frac{a_p}{2\pi}\cdot\arccos\left(\frac{R_i^2 + e^2 - R_t^2}{2eR_i}\right) \tag{5}$$

When $R_i=R_1$, the h_{1211i} and h_{1212i} reach maximum.

$$h_{1211\max} = \frac{a_p}{2\pi}\arccos\left(\frac{R_1^2 + e^2 - R_t^2}{2eR_1}\right) \tag{6}$$

$$h_{1212\max} = \frac{a_p}{2\pi}\cdot\arccos\left(\frac{R_1^2 + e^2 - R_t^2}{2eR_1}\right) \tag{7}$$

Once h_{1211i} and h_{1212i} are known, the cutting depth of periphery cutting edge in region 1 can be obtained.

$$h_{1i} = a_p - h_{1211i} - h_{1212i} \tag{8}$$

Substituting Eqs. (4) and (5) into Eq. (8) gives:

$$h_{1i} = a_p\left(1 - \frac{1}{\pi}\arccos\left(\frac{R_i^2 + e^2 - R_t^2}{2eR_i}\right)\right) \tag{9}$$

The ratio between the decrease along radial direction and the decrease along circumference direction in region 1 (r_{21}) can be expressed as Eq. (10).

$$r_{21} = \frac{h_{1211i}}{h_{1212i}} \Rightarrow r_{21} = 1 \tag{10}$$

Eq. (10) shows that the decrease along the circumference direction and radial direction in region 1 is always the same.

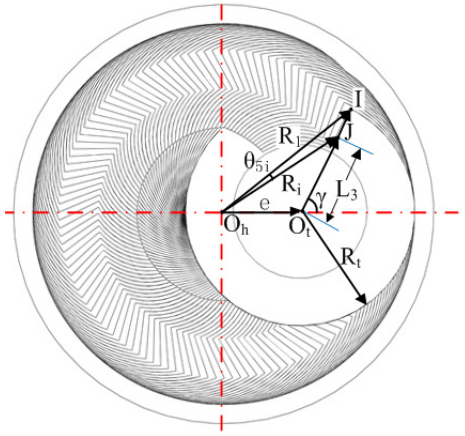

Fig. 11 Schematic diagram for the calculation of L_3 and θ_{5i}

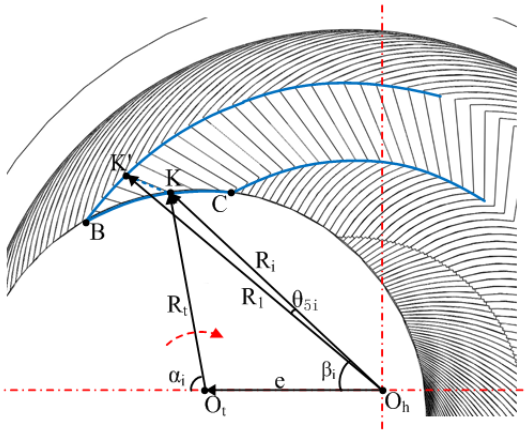

Fig. 12 Graphic for the calculation of h_{1i} in region 2

Region 2: As shown in Fig. 11, the tool mark in region 2 is formed by outside edge. The direction of the tool mark is not along radial direction but has an included angle γ. Point J is the intersection of radius R_i and tool mark. L_3 is the distance from point J to center O_t. The Eq. (11) can be developed according to the law of cosines and geometrical relationships in triangle JO_hO_t.

$$R_i^2 = \mathrm{e}^2 + L_3^2 - 2eL_3\cos(\pi - \gamma) \tag{11}$$

Taking the root of Eq. (11)

$$L_3 = \sqrt{R_i^2 - e^2\sin^2\gamma} - e\cos\gamma \tag{12}$$

The angle θ_{5i} can be obtained according to the geometrical relationships in triangle IJO_h and law of cosines.

$$\theta_{5i} = \arccos\left(\frac{R_1^2 + R_i^2 - \left(R_t - L_3\right)^2}{2R_1 R_i} \right) \tag{13}$$

Once the L_3 and θ_5 are obtained, the decrease along radial direction from B to K (h_{1221i}) can also be obtained (Fig. 12).

$$h_{1221i} = \left(R_t - L_3\right)\tan\theta_1 - a_p \cdot \frac{\theta_{5i}}{2\pi} \tag{14}$$

Substituting Eq. (13) into Eq. (14) gives:

$$h_{1221i} = \left(R_t - L_3\right)\tan\theta_1 - \frac{a_p}{2\pi}\arccos\left(\frac{R_1^2 + R_i^2 - \left(R_t - L_3\right)^2}{2R_1 R_i} \right) \tag{15}$$

The decrease along circumference direction from A to K (h_{1222i}) can be obtained.

$$h_{1222i} = \frac{a_p}{2\pi}\arccos\left(\frac{R_i^2 + e^2 - R_t^2}{2eR_i} \right) \tag{16}$$

When R_i=R_2, the h_{1221i} and h_{1222i} reach maximum.

$$h_{1221\max} = \left(R_t - R_m\right)\tan\theta_1 - \frac{a_p}{2\pi}\arccos\left(\frac{R_1^2 + R_2^2 - \left(R_t - R_m\right)^2}{2R_1 R_2} \right) \tag{17}$$

$$h_{1222\max} = \frac{a_p}{2\pi}\arccos\left(\frac{R_2^2 + e^2 - R_t^2}{2eR_2} \right) \tag{18}$$

Once h_{1221i} and h_{1222i} are known, the cutting depth of periphery cutting edge in region 2 can be obtained.

$$h_{1i} = a_p - h_{1211\max} - h_{1221i} - h_{1222i} \tag{19}$$

The ratio between the decrease along radial direction and the decrease along circumference direction in region 2 (r_{22}) can be expressed as Eq. (20).

$$r_{22} = \frac{h_{1221i}}{h_{1222i} - h_{1212\max}} \tag{20}$$

Substituting Eqs. (7), (15) and (16) into Eq. (20) gives:

$$r_{22} = \frac{\dfrac{2\pi}{a_p}\left(R_t - L_3\right)\tan\theta_1 - \arccos\left(\dfrac{R_1^2 + R_i^2 - \left(R_t - L_3\right)^2}{2R_1 R_i} \right)}{\arccos\left(\dfrac{R_i^2 + e^2 - R_t^2}{2eR_i} \right) - \arccos\left(\dfrac{R_1^2 + e^2 - R_t^2}{2eR_1} \right)} \tag{21}$$

Region 3: In Fig. 13, the point O_m is the center of the circle corresponding arc KK'. The decrease along the radial direction can be replaced by the decrease along circumference direction from K to K' (corresponding to angle θ_{6i}).

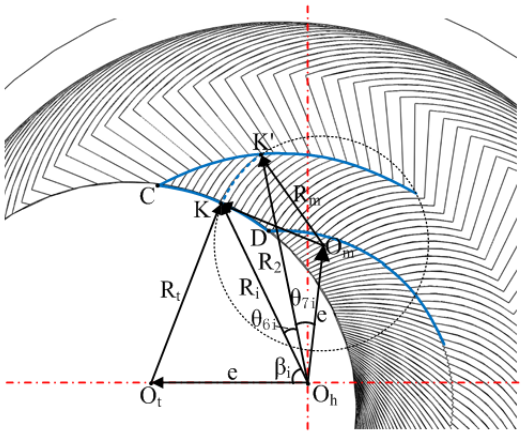

Fig. 13 Graphic for the calculation of periphery cutting depth h_{1i} in region 3

Eq. (22) can be developed according to the geometrical relationships in triangle KO_mO_h.

$$\theta_{6i}+\theta_{7i}=\arccos\left(\frac{R_i^2+e^2-R_m^2}{2eR_i}\right) \tag{22}$$

According to the geometrical relationships in triangle $K'O_mO_h$, the angle θ_{7i} can be obtained:

$$\theta_{7i}=\arccos\left(\frac{R_2^2+e^2-R_m^2}{2eR_2}\right) \tag{23}$$

Thus, substituting Eq. (23) into Eq. (22) gives:

$$\theta_{6i}=\arccos\left(\frac{R_i^2+e^2-R_m^2}{2eR_i}\right)-\arccos\left(\frac{R_2^2+e^2-R_m^2}{2eR_2}\right) \tag{24}$$

After angle θ_{6i} is deduced, the decrease along radial direction from C to K (h_{1231i}) can be obtained.

$$h_{1231i}=a_p\cdot\frac{\theta_{6i}}{2\pi} \tag{25}$$

Substituting Eq. (24) into Eq. (25) gives:

$$h_{1231i}=\frac{a_p}{2\pi}\left[\arccos\left(\frac{R_i^2+e^2-R_m^2}{2eR_i}\right)-\arccos\left(\frac{R_2^2+e^2-R_m^2}{2eR_2}\right)\right] \tag{26}$$

The decrease along circumference direction from A to K (h_{1232i}) can be expressed as following.

$$h_{1232i}=\frac{a_p}{2\pi}\arccos\left(\frac{R_i^2+e^2-R_t^2}{2eR_i}\right) \tag{27}$$

When R_i=R_3, the h_{1231i} and h_{1232i} reach maximum.

$$h_{1231\max}=\frac{a_p}{2\pi}\left[\arccos\left(\frac{R_3^2+e^2-R_m^2}{2eR_3}\right)-\arccos\left(\frac{R_2^2+e^2-R_m^2}{2eR_2}\right)\right] \tag{28}$$

$$h_{1232\max}=\frac{a_p}{2\pi}\arccos\left(\frac{R_3^2+e^2-R_t^2}{2eR_3}\right) \tag{29}$$

Once h_{1231i} and h_{1232i} are known, the cutting depth of periphery cutting edge in region 3 can be obtained.

$$h_{1i}=a_p-h_{1211\max}-h_{1221\max}-h_{1231i}-h_{1232i} \tag{30}$$

The ratio between the decrease along radial direction and the decrease along circumference direction in region 3 can be expressed as Eq. (31).

$$r_{23}=\frac{h_{1231i}}{h_{1232i}-h_{1222\max}} \tag{31}$$

Substituting Eqs. (18), (26) and (27) into Eq. (31) gives:

$$r_{23}=\frac{\arccos\left(\frac{R_i^2+e^2-R_m^2}{2eR_i}\right)-\arccos\left(\frac{R_2^2+e^2-R_m^2}{2eR_2}\right)}{\arccos\left(\frac{R_i^2+e^2-R_t^2}{2eR_i}\right)-\arccos\left(\frac{R_2^2+e^2-R_t^2}{2eR_2}\right)} \tag{32}$$

Region 4: Fig. 14 shows the graphic for the calculation of h_{1i} in region 4. The decrease along the radial direction can be replaced by the decrease along circumference direction from K to K' (corresponding to angle θ_{8i}). According to the geometrical relationship, it's easy to know θ_{8i}=θ_{9i}. Therefore, the decrease of cutting depth along radial direction is equal to the decrease along circumference direction in region 4.

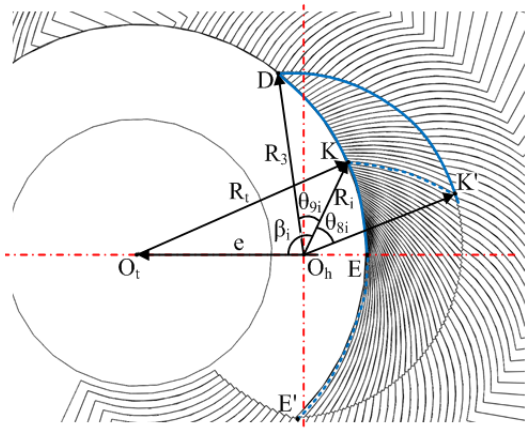

Fig. 14 Graphic for the calculation of inside cutting depth h_{1i} in region 4

The decrease along radial direction from D to K ($h_{1241\mathrm{i}}$) can be expressed as follows.

$$h_{1241i} = a_p \frac{\theta_{8i}}{2\pi} \tag{33}$$

According to the geometrical relationships in Fig. 14, angle $\theta_{8\mathrm{i}}$ can be calculated.

$$\theta_{8i} = \arccos\left(\frac{R_i^2 + e^2 - R_t^2}{2eR_i}\right) - \arccos\left(\frac{R_3^2 + e^2 - R_t^2}{2eR_3}\right) \tag{34}$$

Substituting Eq. (34) into Eq. (33) gives:

$$h_{1241i} = \frac{a_p}{2\pi}\left[\arccos\left(\frac{e^2 + R_i^2 - R_t^2}{2eR_i}\right) - \arccos\left(\frac{e^2 + R_3^2 - R_t^2}{2eR_3}\right)\right] \tag{35}$$

The decrease along circumference direction from A to K ($h_{1242\mathrm{i}}$) can be obtained.

$$h_{1242i} = \frac{a_p}{2\pi}\arccos\left(\frac{e^2 + R_i^2 - R_t^2}{2eR_i}\right) \tag{36}$$

Once $h_{1241\mathrm{i}}$ and $h_{1242\mathrm{i}}$ are known, the periphery cutting depth in region 4 can be obtained.

$$h_{1i} = a_p - h_{1211\max} - h_{1221\max} - h_{1231\max} - h_{1241i} - h_{1242i} \tag{37}$$

The ratio between the decrease along radial direction and the decrease along circumference direction in region 4 can be expressed as Eq. (38).

$$r_{24} = \frac{h_{1241i}}{h_{1242i} - h_{1232\max}} \Rightarrow r_{24} = 1 \tag{38}$$

Therefore, the cutting depth of periphery cutting edge in different regions of condition 2 can be expressed as follows:

$$h_{1i} = \begin{cases} = a_p - h_{1211i} - h_{1212i}, Ri \in [R_1, R_h] \\ = a_p - h_{1211\max} - h_{1221i} - h_{1222i}, R_i \in [R_2, R_1] \\ = a_p - h_{1211\max} - h_{1221\max} - h_{1231i} - h_{1232i}, R_i \in [R_3, R_2] \\ = a_p - h_{1211\max} - h_{1221\max} - h_{1231\max} - h_{1241i} - h_{1242i}, R_i \in [R_t - e, R_3] \end{cases} \tag{39}$$

However, The Eq. (39) requires the value of R_1, R_2, R_3 and γ.

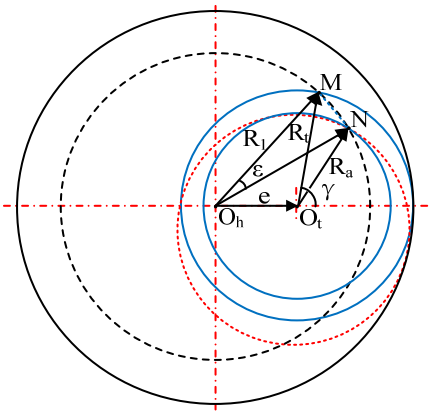

Fig. 15 Schematic diagram for the calculation of radius R_1 and angle γ

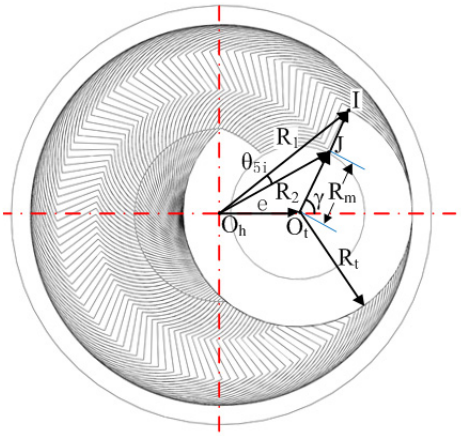

Fig. 16 Graphic for the calculation of radius R_2

As shown in Fig. 15, the large blue circle is trajectory of the highest point on outside cutting edge rotating around the axis of tool and the small blue circle of radius R_a is trajectory of the point which is a feed per tooth lower along axial direction of the hole than the highest point on outside edge. The red dotted circle is the position of the big blue circle rotating around the hole axis about a feed angle of per tooth around the hole axis. The intersection of the small blue circle and the red dotted circle, which is far from the center O_h, is marked N and the value of R_i is equal to the distance between point O_h and point N.

The feed per tooth along axial direction can be calculated by Eq. (40).

$$f_{za} = \frac{a_p \cdot n_g}{N n_z} \tag{40}$$

where n_g is the revolution speed, n_z is the spindle speed, N is the number of tool tooth.

Furthermore, radius of the small blue circle (R_a) can be obtained.

$$R_a = R_t - \frac{f_{za}}{\tan\theta_1} \tag{41}$$

Substituting Eq. (40) into Eq. (41) gives:

$$R_a = R_t - \frac{a_p \cdot n_g}{N n_z \tan\theta_1} \tag{42}$$

The feed angle of per tooth (ε) around the hole axis can be calculated as following.

$$\varepsilon = \frac{2\pi n_g}{n_z N} \tag{43}$$

According to the geometrical relationships in Fig. 15, angle ε can also be expressed as Eq. (44).

$$\varepsilon = \arccos\left(\frac{R_1^2 + e^2 - R_t^2}{2eR_1}\right) - \arccos\left(\frac{R_1^2 + e^2 - R_a^2}{2eR_1}\right) \tag{44}$$

Let Eq. (43) equals to Eq. (44).

$$\frac{2\pi n_g}{n_z N} = \arccos\left(\frac{R_1^2 + e^2 - R_t^2}{2eR_1}\right) - \arccos\left(\frac{R_1^2 + e^2 - R_a^2}{2eR_1}\right) \tag{45}$$

The Eq. (45) contains only variable R_1 and a_p, but it is a transcendental equation which is unable to obtain the analytical solution. Assuming that the R_1 is expressed by a_p with the following equation.

$$R_1 = f\left(a_p\right) \tag{46}$$

Eq. (47) can be developed according to the geometrical relationships in triangle MO_hO_t (Fig. 15).

$$R_1^2 = R_a^2 + e^2 - 2eR_a\cos\left(\pi - \gamma\right) \tag{47}$$

Rewriting Eq. (47):

$$\gamma = \arccos\left(\frac{R_a^2 + e^2 - R_1^2}{-2eR_a}\right) \tag{48}$$

When R_i=R_2, the value of L_3 calculated by Eq. (12) is exactly R_m. Therefore, R_2 can be calculated according to the geometrical relationships in triangle JO_hO_t (Fig. 16) .

$$R_2 = \sqrt{\left(e + R_m\cos\gamma\right)^2 + \left(R_m\sin\gamma\right)^2} \tag{49}$$

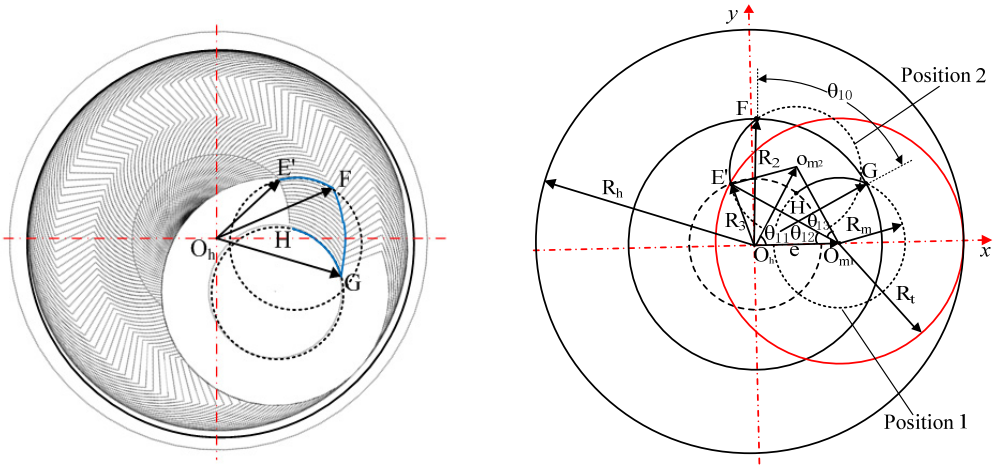

(a) (b)

Fig. 17 Graphic for the calculation of radius R_3: **a** morphology of the uncut material **b** calculation chart

As shown in Fig. 17(a), the altitude intercept between the point E' and H is equal to the height of the outside cutting edge. The decrease of periphery cutting depth from F to G can be calculated using angle θ_{10}. In addition, point E' and F are at the same height, and point H and G are also at the same height. Fig. 17(b) shows the geometrical relationship between the parameters used in calculation of R_3.

Therefore, the following equation can be obtained.

$$\left(R_t - R_m\right)\cdot\tan\theta_1 = a_p\cdot\frac{\theta_{10}}{2\pi} \tag{50}$$

Rewriting Eq. (50):

$$\theta_{10} = \frac{2\pi\left(R_t - R_m\right)\tan\theta_1}{a_p} \tag{51}$$

The angle from position 1 to position 2 (θ_{11}) can be expressed as Eq. (52).

$$\theta_{11} = \theta_{10} \Rightarrow \theta_{11} = \frac{2\pi\left(R_t - R_m\right)\tan\theta_1}{a_p} \tag{52}$$

In isosceles triangle $O_{m2}O_hO_{m1}$, the length of O_hO_{m1} is equal to the length of O_hO_{m2} and Eq. (53) can be derived.

$$\theta_{12} + \theta_{13} = \frac{\pi - \theta_{10}}{2} \tag{53}$$

The distance between center O_{m1} and O_{m2} can be calculated when the angle θ_{10} is known.

$$L_{O_{m2}O_{m1}} = e\cdot\sqrt{2\left(1-\cos\theta_{10}\right)} \tag{54}$$

Furthermore, the angle θ_{13} can be calculated because the three sides of the triangle $O_{m2}E'O_{m1}$ are known.

$$\theta_{13}=\arccos\left(\frac{2e^2\left(1-\cos\theta_{10}\right)+R_t^2-R_m^2}{2eR_t\sqrt{2\left(1-\cos\theta_{10}\right)}}\right) \tag{55}$$

Substituting Eq. (55) into Eq. (53) gives:

$$\theta_{12}=\frac{\pi-\theta_{10}}{2}-\arccos\left(\frac{2e^2\left(1-\cos\theta_{10}\right)+R_t^2-R_m^2}{2eR_t\sqrt{2\left(1-\cos\theta_{10}\right)}}\right) \tag{56}$$

The R_3 can be calculated according to the geometrical relationships in triangle EO_hO_{m1} and law of cosines.

$$R_3=\sqrt{R_t^2+e^2-2eR_t\cos\left(\frac{\pi-\theta_{10}}{2}-\arccos\left(\frac{2e^2\left(1-\cos\theta_{10}\right)+R_t^2-R_m^2}{2eR_t\sqrt{2\left(1-\cos\theta_{10}\right)}}\right)\right)} \tag{57}$$

Substituting Eq. (51) into Eq. (57) gives:

$$R_3=\sqrt{R_t^2+e^2-2eR_t\cos\left(\frac{\pi}{2}-\frac{\pi\left(R_t-R_m\right)\tan\theta_1}{a_p}-\arccos\left(\frac{2e^2\left(1-\cos\left(\frac{2\pi\left(R_t-R_m\right)\tan\theta_1}{a_p}\right)\right)+R_t^2-R_m^2}{2\sqrt{2}eR_t\sqrt{1-\cos\left(\frac{2\pi\left(R_t-R_m\right)\tan\theta_1}{a_p}\right)}}\right)\right)} \tag{58}$$

The a_{p1} is the boundary value for morphology of uncut material from condition 1 to condition 2. Assuming that the region 4 exists and the value R_3 can be calculated. However, the region 4 is very small and cut by the outside cutting edge, so the region 4 can't be seen in condition 1. With the increase of value a_p, the value of R_3 also increase. When the R_3 reaches R_t-e, the value of a_p is the boundary value a_{p1}.

Substituting R_3=R_t-e into Eq. (58) and the value a_{p1} can be calculated. However, the explicit solution of a_{p1} can't be derived because the Eq. (58) is a transcendental equation. Assume that the a_{p1} is expressed as following.

$$a_{p1}=f_2\left(R_t,R_m,R_h\right) \tag{59}$$

The a_{p2} is the boundary value for morphology of uncut material from condition 2 to condition 3. When circle O_m and O_t are interior contact (Fig. 18), the value of a_p is the maximum that can be sustained in condition 2. In this case, the minimum of angle θ_{10} can be obtained.

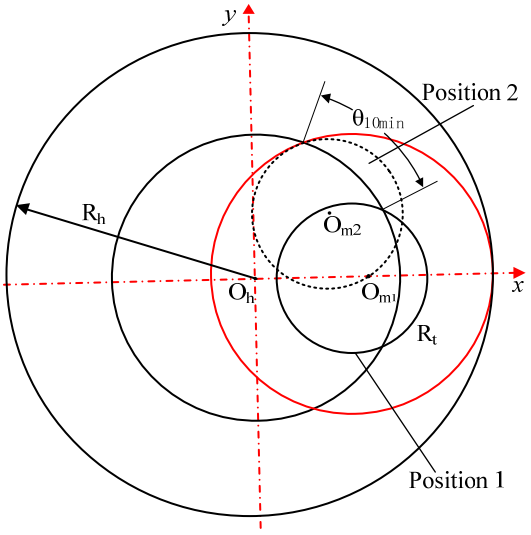

Fig. 18 Schematic diagram for the calculation of boundary value a_{p2}

$$\theta_{10\min} = \arccos\left(\frac{2e^2 - \left(R_t - R_m\right)^2}{2e^2}\right) \tag{60}$$

Substituting Eq. (60) into Eq. (51) gives:

$$a_{p2} = \frac{2\pi\left(R_t - R_m\right)\tan\theta_1}{\arccos\left(\frac{2e^2 - \left(R_t - R_m\right)^2}{2e^2}\right)} \tag{61}$$

3.1.3 The third type of uncut material morphology (condition 3)

In this condition, the helicoid is divided into three regions and region 3 disappears compared with condition 2 (Fig. 19). The calculation method of the cutting depth is similar to the condition 2 and the analysis and calculating process is not repeated here.

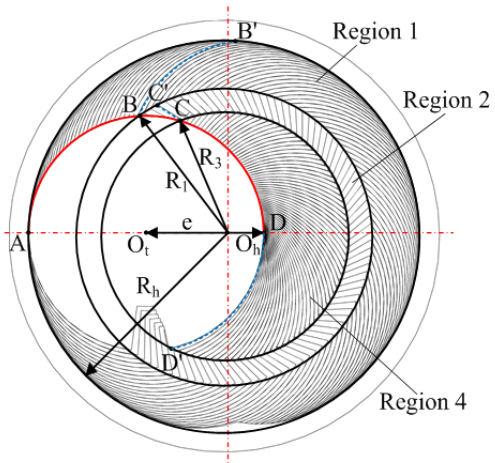

Fig. 19 Regional division of the uncut material in condition 3

3.1.4 The fourth type of uncut material morphology (condition 4)

In this condition, the helicoid contains only one region (Fig. 20). Therefore, the periphery cutting depth is easy to calculate and can be expressed as following.

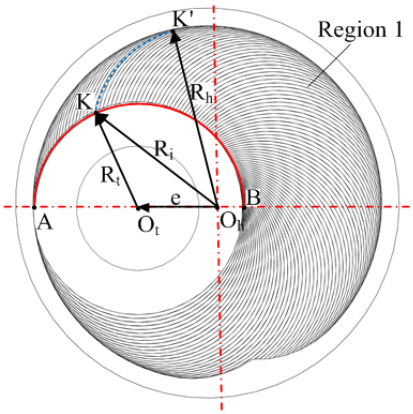

Fig. 20 Regional division of the uncut material in condition 4

$$h_{14i} = a_p\left[1-\frac{1}{\pi}\arccos\left(\frac{e^2+R_i^2-R_t^2}{2eR_i}\right)\right], R_i \in \left[R_t-\mathrm{e}, R_\mathrm{h}\right] \tag{62}$$

3.2 Cutting depth of inside cutting edge

The cutting depth of the inside edge (h_{2i}) is easier to calculate than the cutting depth of the periphery cutting edge (h_{1i}). As mentioned above, the formula of periphery cutting depth varies when the morphology of uncut material changes. However, the calculation method of inside cutting depth remains unchanged no matter what the morphology of uncut material is.

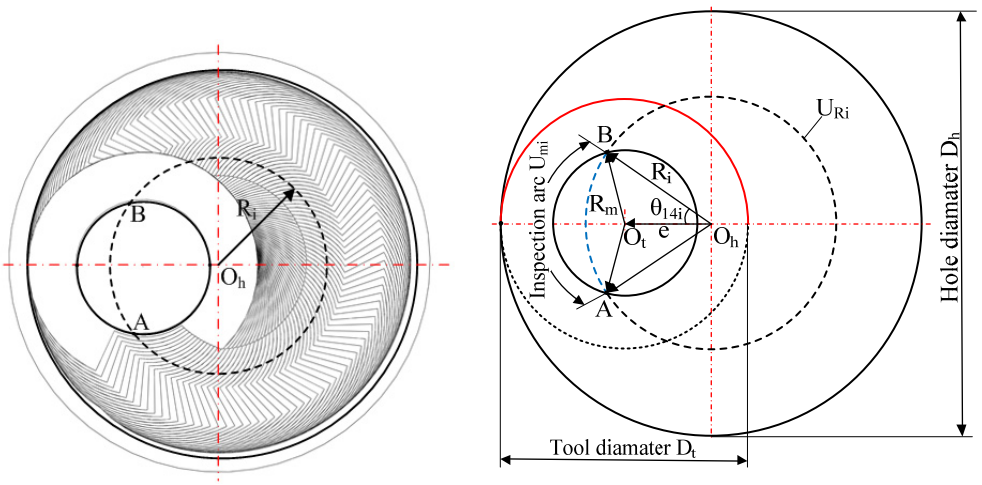

(a) (b)

Fig. 21 Graphic for the calculation of inside cutting depth h_{2i}: **a** morphology of the uncut material **b**

calculation diagram

The cutting depth of inside edge (h_{2i}) can be developed with the projected tool path triangle on the arbitrary inspection radius R_i (Fig. 21) [15].

$$\frac{h_{2i}}{U_{m_i}} = \frac{a_p}{U_{R_i}} \Rightarrow h_{2i} = a_p \cdot \frac{U_{m_i}}{U_{R_i}} \tag{63}$$

Eq. (63) describes the geometric dependence of the inside cutting depth (h_{2i}) on the arc length of the full circle with radius R_i, the depth setting per orbital path (a_p) and the inspection arc (U_{mi}). The value of U_{mi} and U_{Ri} can be expressed as following.

$$U_{mi} = 2\theta_{14i} R_i \tag{64}$$

$$U_{Ri} = 2\pi R_i \tag{65}$$

Substituting Eqs. (64) and (65) into Eq. (63) gives:

$$h_{2i} = a_p \cdot \frac{\theta_{14i}}{\pi} \tag{66}$$

According to the geometrical relationships in triangle BO_hO_t and combined with the law of cosines, the angle θ_{14i} can be derived.

$$\theta_{14i} = \arccos\left(\frac{R_i^2 + e^2 - R_m^2}{2eR_i} \right) \tag{67}$$

Substituting Eq. (67) into Eq. (66) gives:

$$h_{2i} = \frac{a_p}{\pi} \arccos\left(\frac{R_i^2 + e^2 - R_m^2}{2eR_i} \right) \tag{68}$$

Eq. (68) describes the relationship between the cutting depth of inside edge (h_{2i}) and depth setting of the helical course (a_p). The value of h_{2i} changes lineally with a_p.

3.3 Cutting depth of outside cutting edge

As shown in Fig. 22, the uncut material is divided into four zones according to the kinds of cutting edges participating in milling process. In zone 1, the periphery cutting edge and outside edge participate in cutting process together (Fig. 23(a)). In zone 2, the three kinds of cutting edges all participate in milling process (Fig. 23(b)). In zone 3, the outside cutting edge and inside cutting edge participate in milling process together (Fig. 23(c)). In zone 4, only the outside cutting edge participates in milling process (Fig. 23(d)).

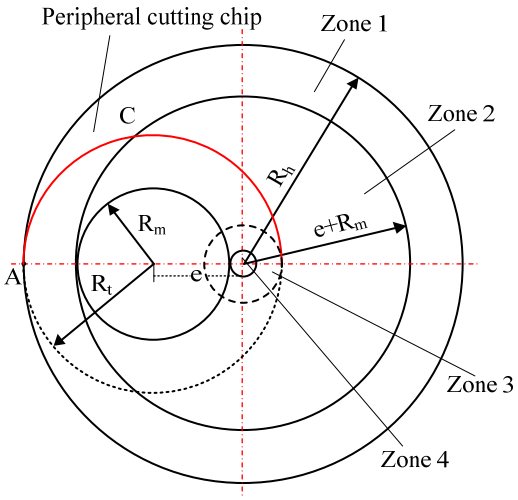

Fig. 22 Area partition of the uncut material according to the participating edges

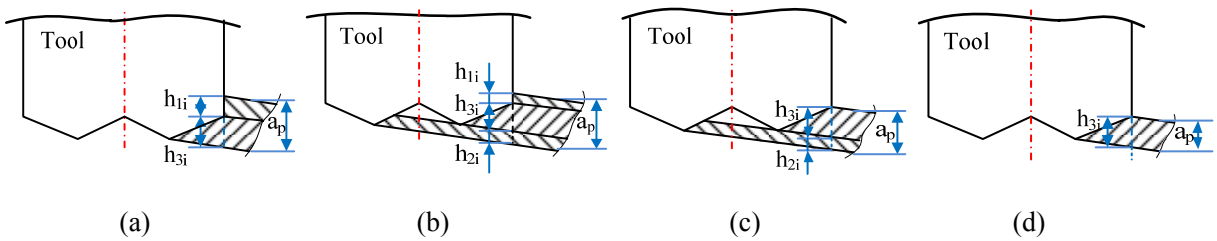

Fig. 23 Type of cutting edges in different zones: **a** zone 1 **b** zone 2 **c** zone 3 **d** zone 4

Assuming that h_{1i} and h_{2i} are known, the cutting depth of outside edge (h_{3i}) can be calculated with the following equation.

$$h_{3i} = \begin{cases} a_p - h_{1i}, R_i \in [e + R_m, R_h] \\ a_p - h_{1i} - h_{2i}, R_i \in [R_t - e, e + R_m] \\ a_p - h_{2i}, R_i \in [e - R_m, R_t - e] \\ a_p, R_i \in [0, e - R_m] \end{cases} \tag{69}$$

4 Effects of the depth setting of the helical course (a_p) and eccentricity (e) on cutting depths (h_{1i}, h_{2i}, h_{3i})

The morphology of uncut material may be different with varying cutting parameters. To some extent, it also reflects the variation of the cutting depths. The effects of depth setting of the helical course (a_p) on morphology of uncut material have been mentioned above (Fig. 6), four kinds of morphologies will appear with the increase of a_p. The impact of eccentricity (e) on morphology of uncut material is shown in Fig. 24. When the value of a_p is kept unchanged, the morphology of

uncut material changes with the increase of eccentricity (e) from a small value to a large value. Furthermore, the morphology formed by the tool belongs to the four kinds of morphology mentioned above. Therefore, the calculation methods of cutting depths (h_{1i}, h_{2i}, h_{3i}) are also useful. In order to find out the relationships between the cutting depths (h_{1i}, h_{2i}, h_{3i}) and the cutting parameters (a_p, e), the calculation of cutting depths was made with constant cutting parameters in table 1.

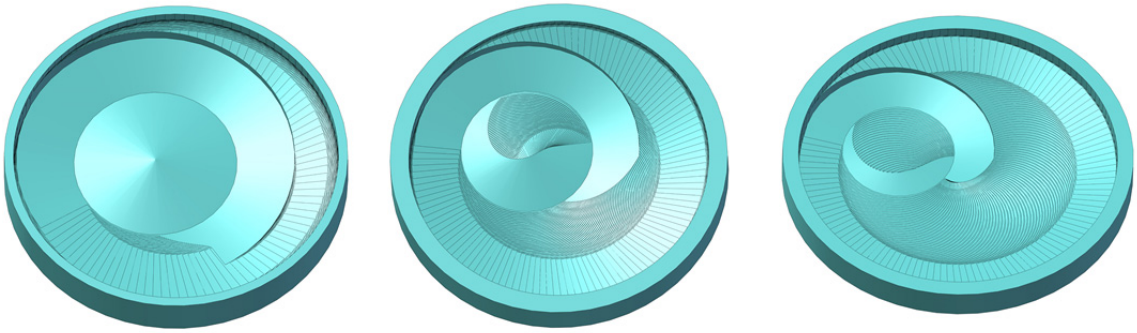

(a) (b) (c)

Fig. 24 Morphology of the uncut material under different eccentricity e (a_p=0.4 mm/r): **a** e=0.5 mm **b** e=1 mm **c** e=2 mm

Table 1 Cutting parameters and tool structure

R_t (mm)	R_m (mm)	θ_l (°)	N	n_z (r/min)	n_g (r/min)
3	1.76	8.32	4	25.64	1500

The effects of the depth setting of the helical course (a_p) and eccentricity (e) on periphery cutting depth (h_{1i}) are given in Fig. 25. The red, green, blue and black curves show the variation of periphery cutting depth with R_i under different morphology of uncut material respectively (conditions 1, 2, 3 and 4). As shown in Fig. 25(a), when the eccentricity (e) is kept constant, it can be seen that the change rule of h_{1i} is a little different with various a_p. When the a_p is small, the h_{1i} decreases with the decrease of R_i at an almost constant change rate in the right part of the curve and at a smaller constant change rate in the left part. It is also noteworthy that the value of R_i corresponding to h_{1i}=0 decreases with the increase of a_p, which means that the length of the periphery cutting chip increases with the increase of a_p. When the a_p is large, the h_{1i} decreases sharply with a gradually reductive change rate when the value of R_i decreases in the right part of the curve. However, in the middle part of the curve, the h_{1i} decreases almost linearly. Then, the

changes rate increases rapidly with the decrease of R_i at the left part of the curve. It also can be observed that the third type of morphology of uncut material appears only in a very narrow interval of a_p. When compared the change rules of h_{1i} with different value of e (e=2, e=1, e=0.5), it can be found that the width of interval of a_p ,in which the second type of morphology appears, decreases gradually (see Fig. 25(b)) and becomes zero (see Fig. 25(c)) at some point with the value of e reducing. The fourth type of morphology will appear at a lower and lower value of a_p with the decrease of e.

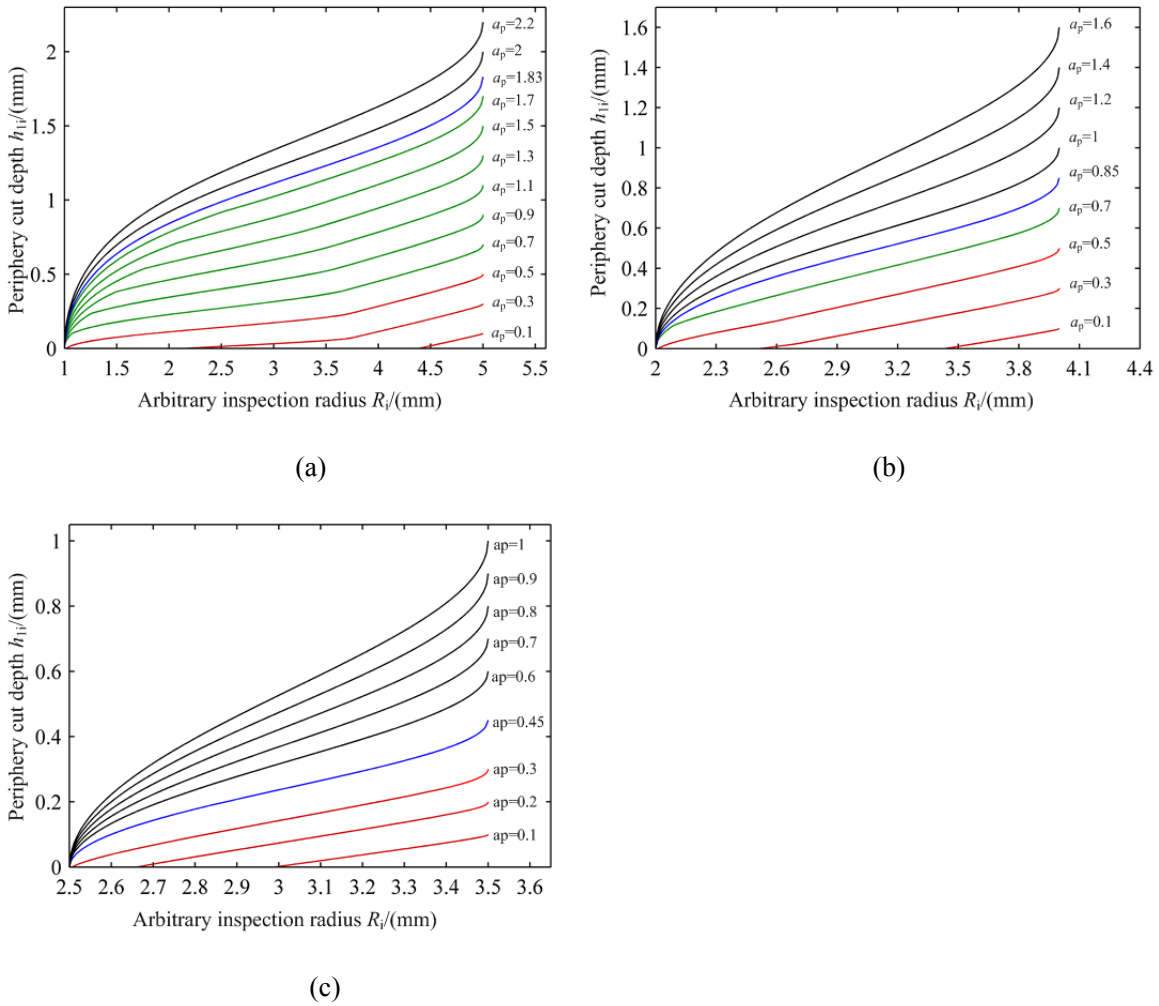

Fig. 25 Variation of periphery cutting depth h_{1i} under different a_p and e: **a** e=2 **b** e=1 **c** e=0.5

The effects of the depth setting of the helical course (a_p) and eccentricity (e) on inside cutting depth (h_{2i}) are also provided based on the established models. Fig. 26(a) shows the influence of a_p on inside cutting depth when e takes a large value. It can be seen that the h_{2i} increases with the increase of a_p. The h_{2i} on both ends of curves is zero and sharply increases from the ends to the middle part of curves. The maximum of h_{2i} appears near R_i=1, which is not in the middle of curves. This phenomenon is caused by two reasons: one reason is that the change rate of cutting depth

along circumferential direction（$a_p/2\pi R_i$）increases gradually when the R_i changes from R_h to 0; the other reason is that the length of the inspection arc U_{mi} first increases and then decreases when the R_i changes from R_h to 0. Fig. 26(c) shows the influence of a_p on inside cutting depth when e takes a small value. It can be seen that the h_{2i} increases significantly till reaching maximum and keeps unchanged when R_i changes from a large value to zero. When compared the change rules of h_{2i} with different value of e (e=2, e=1, e=0.5), it can be found that the cutting area of inside edge decreases with the decrease of e, the material near the center of hole will be removed completely by inside edge when e takes a small value. Therefore, the h_{2i} equals to the value of a_p in the area near the center of hole.

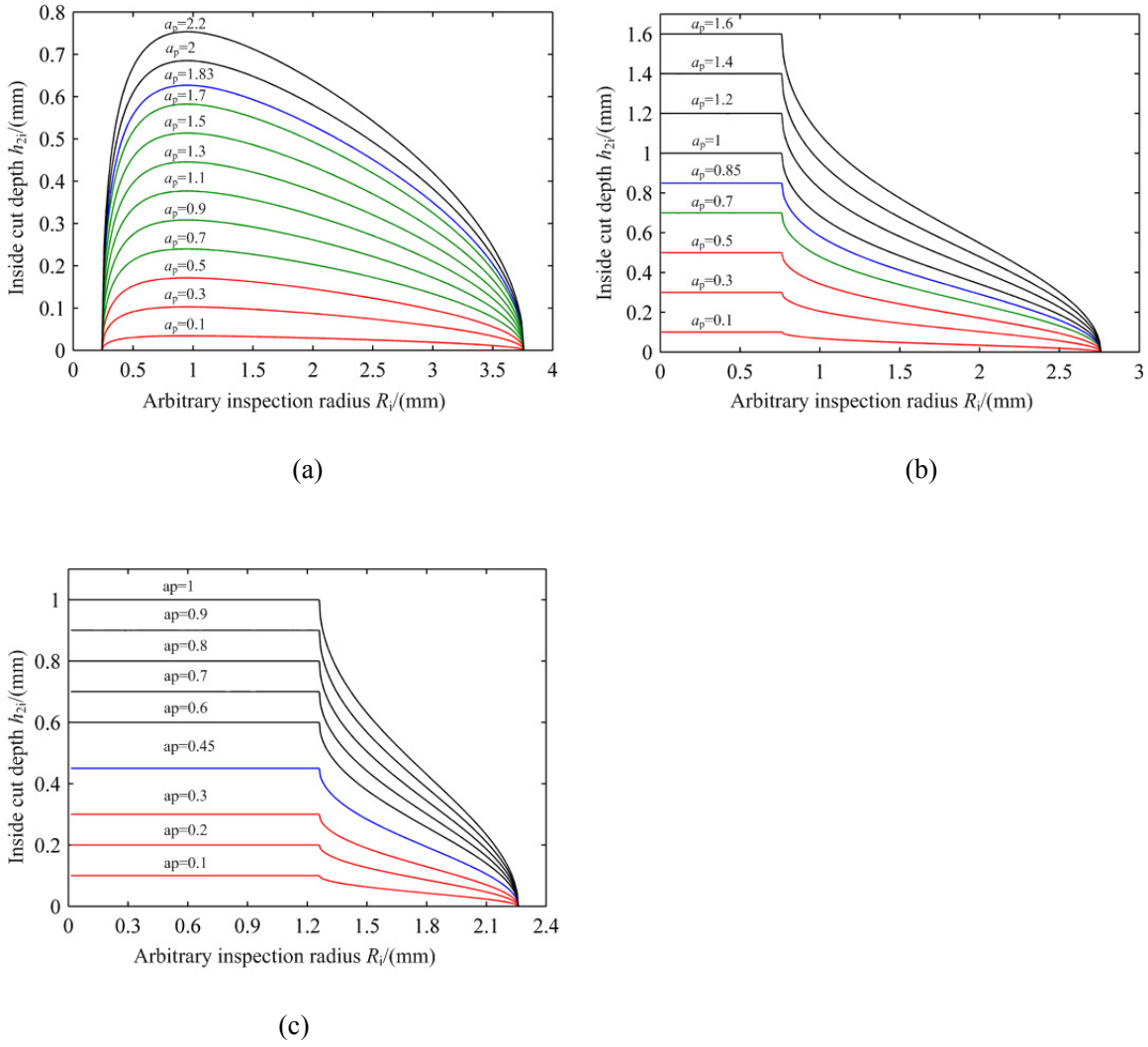

(a) (b)

(c)

Fig. 26 Variation of inside cutting depth h_{2i} under different a_p and e: **a** e=2 **b** e=1 **c** e=0.5

Fig. 27 shows the curves of outside cutting depth (h_{3i}) with different value of a_p and e. The curves of h_{3i} are a little complex when compared with the curves of h_{1i} and h_{2i}. When the e is kept

constant, the h_{3i} changes gently with a small value of ap and the change rate of h_{3i} increases with the increase of a_p. When compared the change law of h_{3i} with different value of e (e=2, e=1, e=0.5), it can be found that the curve pattern varies significantly, one reason is that the cutting area of cutting edges changes with the variation of e.

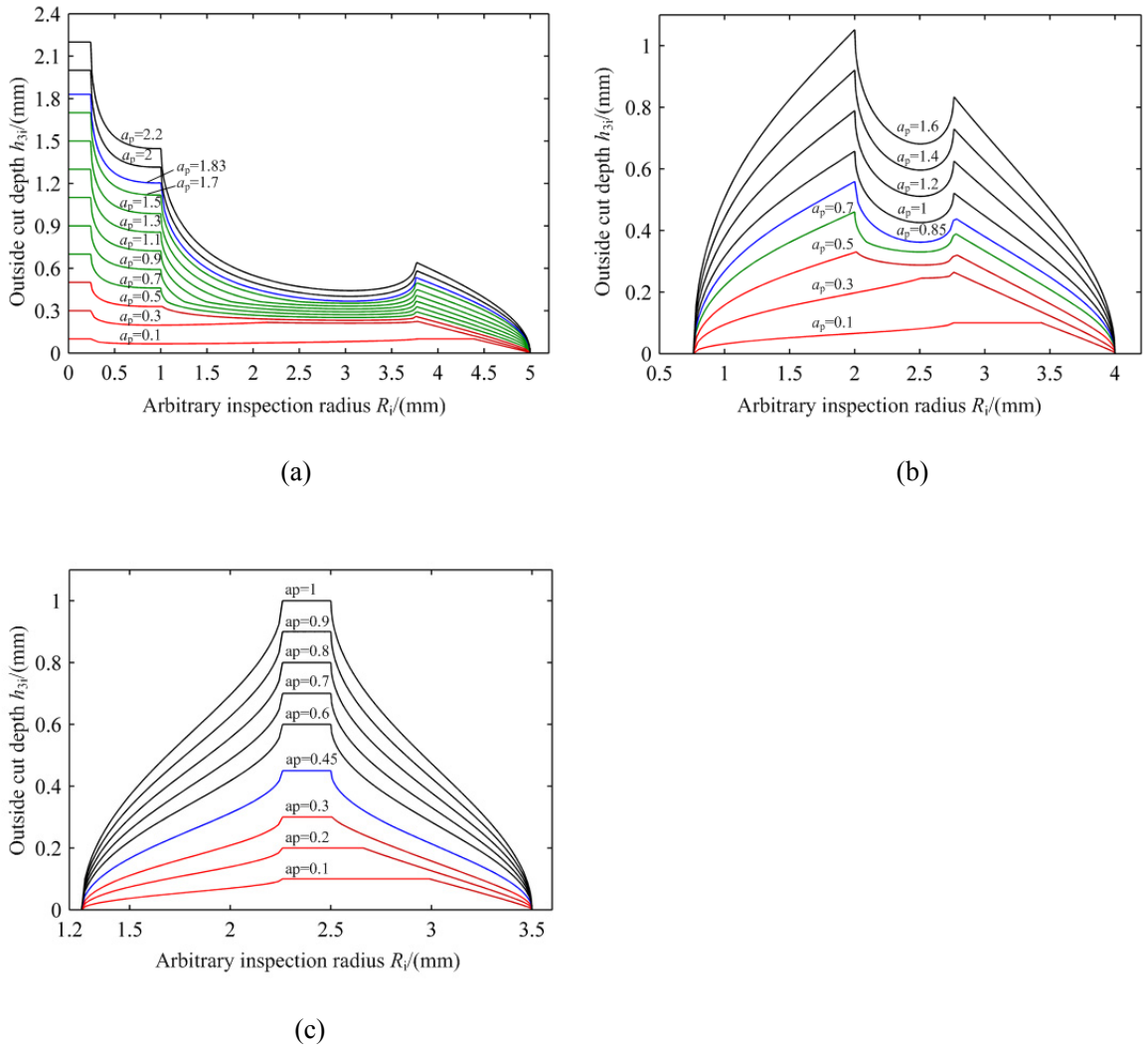

Fig. 27 Variation of outside cutting depth h_{3i} under different a_p and e: **a** e=2 **b** e=1 **c** e=0.5

5 Cut volume and cut volume ratio

The changes of cut volume of cutting edges will influence the cutting conditions such as chattering, variation of the cutting forces and the deformation degree of cutting tool. Therefore, the cut volumes of the periphery cutting edge (V_1), the inside cutting edge (V_2), the outside cutting edge (V_3) are calculated respectively and then the cut volume ratios are derived.

5.1 Cut volume of the periphery cutting edge

On the thin wall cylinder of radius R_i, the cutting area of the periphery cutting edge in one

orbital revolution can be expressed as following.

$$A_{1i} = 2\pi \cdot R_i \cdot h_{1i} \tag{70}$$

Assuming that the periphery cutting edge participates in cutting in the range of $R_i \in [R_0, R_h]$, the volume removed by the periphery cutting edge (V_1) is given by the summation of all partial areas over the radius $R_i \in [R_0, R_h]$. The cut volume V_1 in one orbital revolution can be obtained by integrating the A_{1i} in the range of $R_i \in [R_0, R_h]$.

$$V_1 = 2\pi \int_{R_0}^{R_h} h_{1i} \cdot R_i \cdot dR_i \tag{71}$$

5.2 Cut volume of the inside edge

On the thin wall cylinder of radius R_i, the cutting area of the inside edge in one orbital revolution can be expressed as following.

$$A_{2i} = 2\pi \cdot R_i \cdot h_{2i} \tag{72}$$

The inside edge participates in cutting in the range of $R_i \in [e\text{-}R_m, e\text{+}R_m]$, the volume removed by the inside edge (V_2) is given by the summation of all partial areas over the radius $R_i \in [e\text{-}R_m, e\text{+}R_m]$. The cut volume V_2 in one orbital revolution can be obtained by integrating the A_{2i} in the range of $[e\text{-}R_m, e\text{+}R_m]$.

$$V_2 = 2\pi \int_{e-R_m}^{e+R_m} h_{2i} \cdot R_i \cdot dR_i \tag{73}$$

5.3 Cut volume of the outside edge

Direct solution of the cut volume of the outside edge (V_3) is a little complicated. Therefore, it is obtained by subtracting the volume removed by the periphery cutting edge (V_1) and inside edge (V_2) from the total volume removed by all cutting edges (V) in one orbital revolution.

The cut volume V and V_3 can be expressed as following:

$$V = \pi \cdot R_h^2 \cdot a_p \tag{74}$$

$$V_3 = V - V_1 - V_2 \tag{75}$$

Substituting Eqs. (71) , (73) and (74) into Eq. (75) gives:

$$V_3 = \pi \cdot R_h^2 \cdot a_p - 2\pi \int_{R_0}^{R_h} h_{1i} \cdot R_i \cdot dR_i - 2\pi \int_{e-R_m}^{e+R_m} h_{2i} \cdot R_i \cdot dR_i \tag{76}$$

Fig. 28 shows the impact of a_p on cutting volume V_1, V_2, V_3. When a_p changes from 0.1 mm/r to 2.2 mm/r, the V_1 increases almost linearly as a whole, the change rate of V_1 is a little lower when

the a_p is small than a_p is large. The V_2 changes linearly with the a_p and this result can also be deduced from Eqs. (68) and (73). When the a_p changes from small to large, the V_3 increases with a large rate first and then increases with a smaller rate when the a_p beyond a critical value. (Fig. 28(c)).

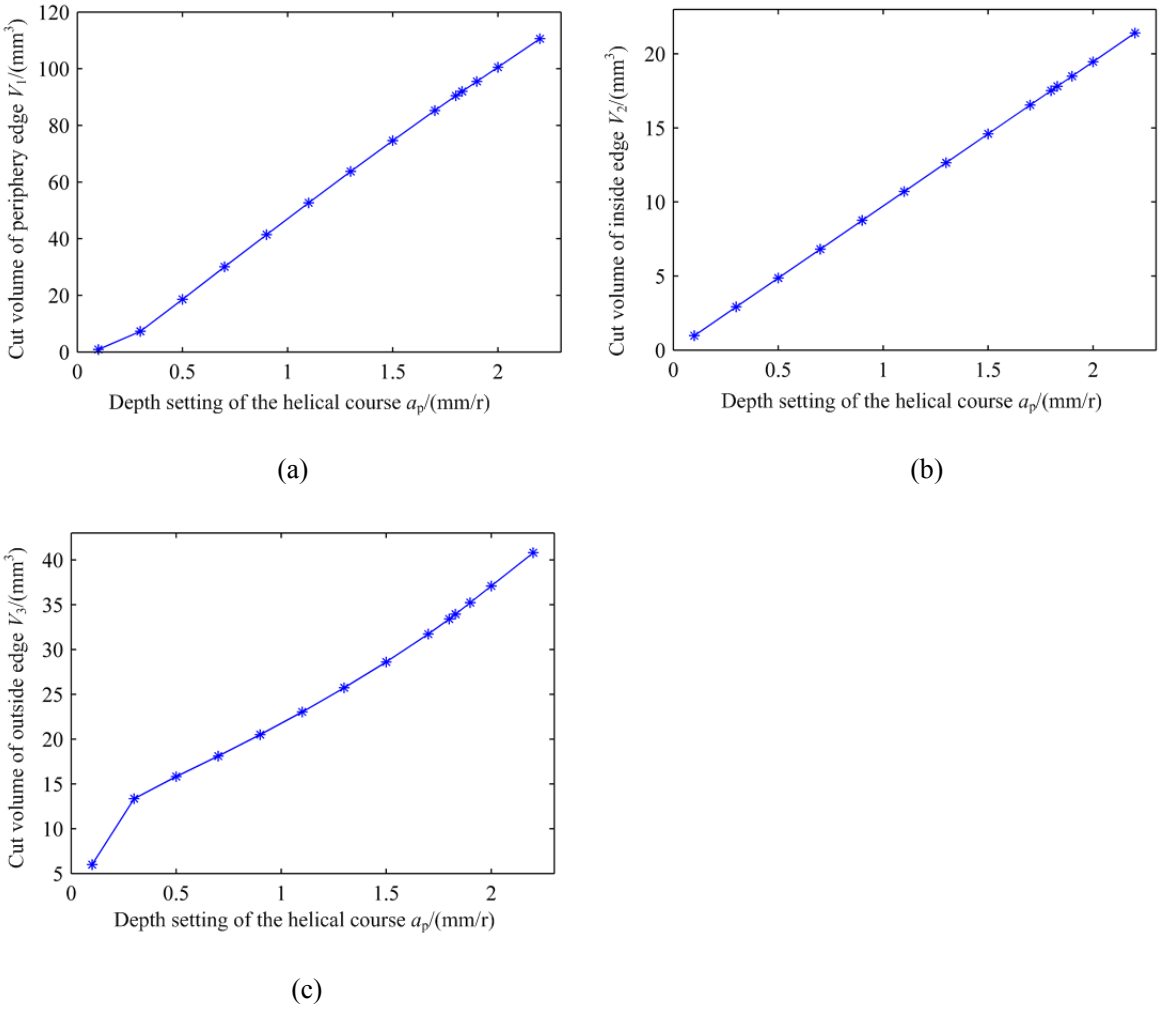

Fig. 28 Variation of cut volume under different depth setting of the helical course a_p (e=2): **a** V_1 **b** V_2 **c** V_3

5.4 The ratio (G) between periphery cut volume and front cut volume

In helical milling process, the different cutting edges will produce different types of cutting force. The periphery cutting edge produces mainly radial cutting force; the front cutting edge produces not only radial cutting force but axial cutting force. The radial cutting force may lead to radial deflection of the tool and cause vibration, the axial cutting force may make the workpiece deform in axial direction of machining hole and lead to poor surface integrity.

The ratio G can reflect the distribution of the cutting forces along radial direction and circumferential direction to some extent. Therefore, it's necessary to study the influence of the

parameters on the ratio G between periphery cut volume (V_1) and front cut volume (V-V_1). The ratio G can be calculated as follows.

$$G=\frac{V_1}{V-V_1} \tag{77}$$

Fig. 29 shows the impact of the depth setting of the helical course (a_p) and eccentricity (e) on the ratio G. It can be seen that the calculated ratio G is in good agreement with that of measured in Solidworks. The slight difference may be due to the modeling error in Solidworks, approximate calculation in Matlab.

When the e is kept unchanged and the a_p takes a small value, the ratio G is very low, which indicates that most of the hole volume is removed by inside and outside cutting edge. With the a_p increasing, the ratio G increases and reaches maximum when a_p exceeds a certain threshold, which means that the ratio G can only changes in a limited range and can't increase without limit. When e takes value 2, 1, 0.5, the maximum of ratio G are 1.78, 0.78 and 0.36 respectively. It can be seen that the maximum of ratio G decreases when the e changes from small to large. The change interval of ratio G becomes more and more smaller with the decrease of e. It is remarkable that the maximum of ratio G equals to the ratio between the periphery and front cut volume removed by conventional end mill over one orbital revolution.

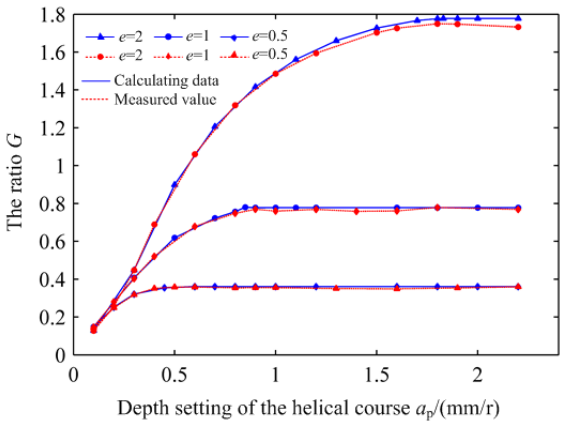

Fig. 29 Variation of the ratio G under different a_p and e

5.5 The ratio (G_1 G_2 G_3) between the cut volume of cutting edges and the total hole volume

All cutting edges are directly involved in helical milling process and a strong interaction will happen between tool and workpiece. The cutting edges will wear gradually with the cut volume increasing. Tool failure occurs once the wear condition of any edge reaches the critical value. However, some edges wear sharply, but some edges wear slightly in helical milling process, which

may lead to varying degree of wear on different edges.

Therefore, it's essential to find out the ratio between the volume removed by periphery cutting edge and the total hole volume (G_1), the ratio between the volume removed by inside edge and the total hole volume (G_2), the ratio between the volume removed by outside edge and the total hole volume (G_3). The ratio G_1, G_2, G_3 can be calculated as follows.

$$G_1 = \frac{V_1}{V} \tag{78}$$

$$G_2 = \frac{V_2}{V} \tag{79}$$

$$G_3 = \frac{V_3}{V} \tag{80}$$

Simulations under different cutting parameters were carried out to reveal the impact of the depth setting of the helical course (a_p) and eccentricity (e) on the ratio G_1, G_2, G_3, and the results were shown in Fig.30. It can be seen that the calculated ratio G_1, G_2, G_3 are in good agreement with that of measured in Solidworks.

As shown in Fig. 30(a), it is easy to be found that the ratio G_1 increases remarkably with the increase of a_p and reaches maximum when a_p beyond some certain value. The ratio G_2 stays constant no matter what value of the a_p is. The ratio G_3 decreases with the a_p changing from small to large and reaches minimum when a_p beyond some certain value. When the curves of ratio G_1 G_2 G_3 with different value of e are compared, it can be found that the maximum of ratio G_1 decreases gradually with the decrease of e. However, the value of ratio G_2 and the minimum of ratio G_3 increase with the decrease of e. When e takes a large value (Fig. 30(a)(b)), the volume removed by outside edge is larger than the volume removed by periphery cutting edge with a small value of a_p and smaller than the volume removed by periphery cutting edge with a large value of ap. When e takes a small value (Fig. 30(c)), the volume removed by outside cutting edge is always larger than the volume removed by periphery cutting edge no matter what value of a_p is.

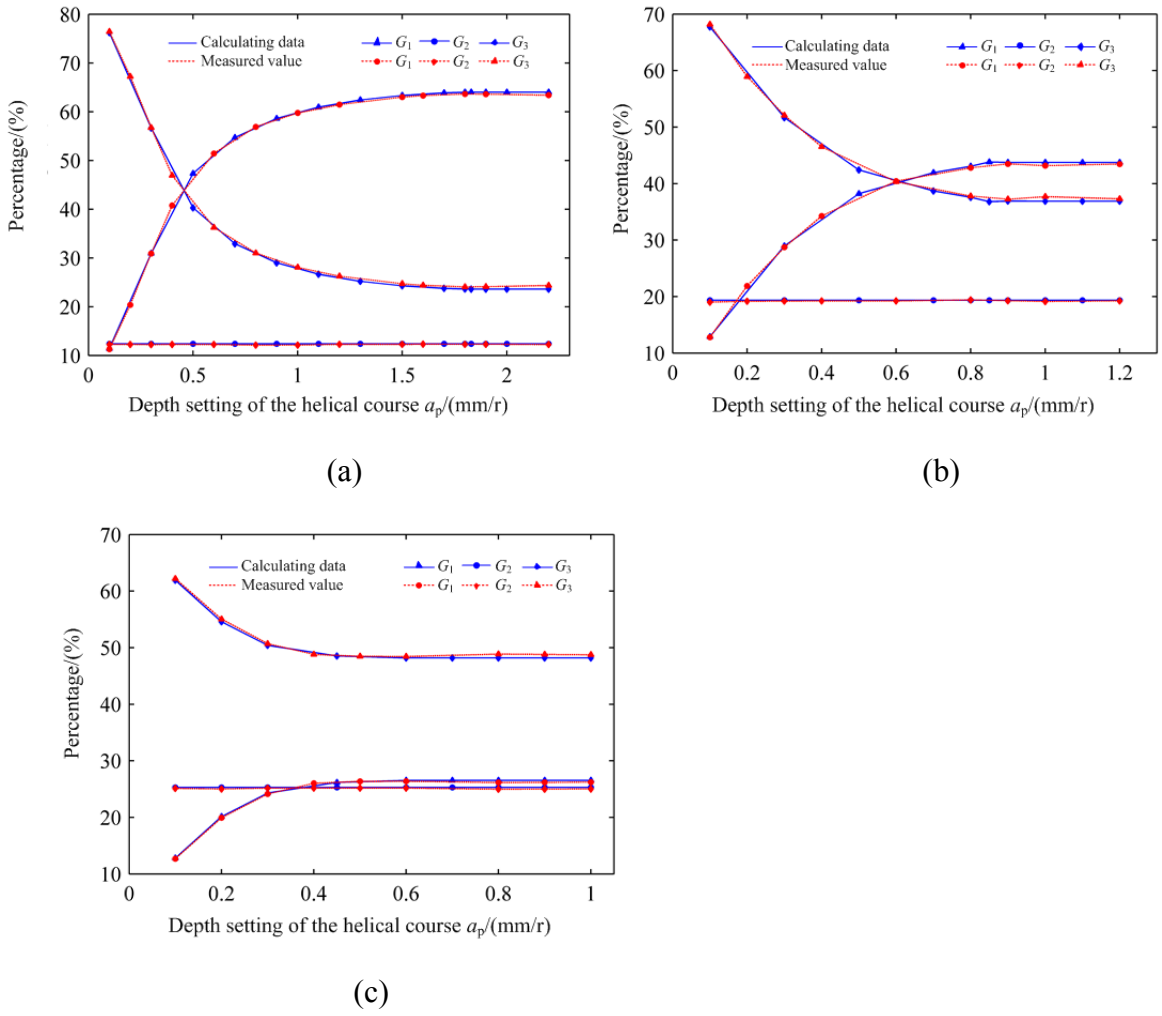

Fig. 30 Variation trends of G_1, G_2, G_3 under different a_p and e: **a** e=2 **b** e=1 **c** e=0.5

6 Undeformed chip geometry during helical milling processes

In actual manufacturing process，the undeformed chip geometry is an indicator which should be treated carefully. On the one hand, it can reflect the working intensity of the different parts on the cutting edge and evaluate the wear rate of the cutting edge. On the other hand, the size of undeformed chip will influence the degree of difficulty of chip removal. The machined surface may be scratched when the size of undeformed chip is large, which will reduce the quality of machined surface. In addition, the deformation degree of cutting chip changes with different morphology of cutting chip and too large deformation degree will lead to unfavorable situations, such as the increase of power dissipation and cutting force. Therefore, it is necessary to study the relationships between the morphology of undeformed chip and the cutting parameters.

The undeformed chip geometry of the helical milling specialized tool is shown in Fig. 31. Three kinds of chip can be seen in picture: the chip formed by periphery cutting edge has a small

width and height but a large length (part in blue); the chip formed by outside cutting edge has a small height but a large width and length, which looks like a fan. Be similar to the morphology of chip formed by outside edge, the geometry of the inside cutting chip also looks like a fan, but the size of it is smaller than the former. It can also be found that the connection between the chips of inside edge and outside edge is weak, which will break easily and facilitates chip removal effectively.

The impact of the depth setting of the helical course (a_p) on the undeformed chip geometry is given in Fig. 32. The width of undeformed periphery chip stays the same, but the length and height increase sharply when a_p changes from a small value to a large one, the maximum that the length can reaches is πR_t. The width, length and width of undeformed inside chip increase with the increase of ap, but the length-width ratio decreases. As for undeformed outside chip, the length of it increases slowly with a_p increasing. When a_p takes small value, width of a part of the chip reaches maximum and the width of last part is still small. The proportion of part where the width reaches maximum increases when the a_p takes a larger value. From the Fig. 32, it can also be found that the length of the connection between the chips of inside edge and outside edge becomes larger and larger, which may lead to a difficulty in separating.

The influence of the eccentricity (e) on the undeformed chip geometry is given in Fig. 33. The length of periphery chip decreases when e changes from small to large, the width and height keep unchanged. The length and width of inside chip decrease and length-width ratio increases with the increase of e. When e=0.5 and e=1, the width of right part of the inside chip is larger than the width of left part obviously. One reason is that the material in the middle of hole is removed by inside cutting edge completely. The length of outside chip decreases with the increase of e and the proportion of part where the width reaches maximum also decrease. It is also worth noting that the length of the connection between the chips of inside edge and chip of outside edge becomes smaller and smaller, which improves the chip removal condition.

The study on relationships between the undeformed chip geometry and cutting parameters (a_p and e) are profitable. It is conducive to optimize machining parameters of helical milling and helpful to improve the tool life. Structure of the tool has a significant influence on chip morphology. Therefore, the research of undeformed chip geometry is useful to assist the design of helical milling specialized tool and can make the structure more suitable for helical milling method.

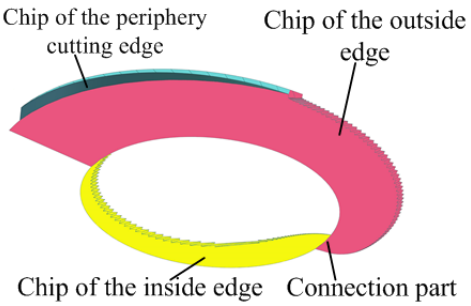

Fig. 31 Undeformed chip geometry formed by helical milling specialized tool

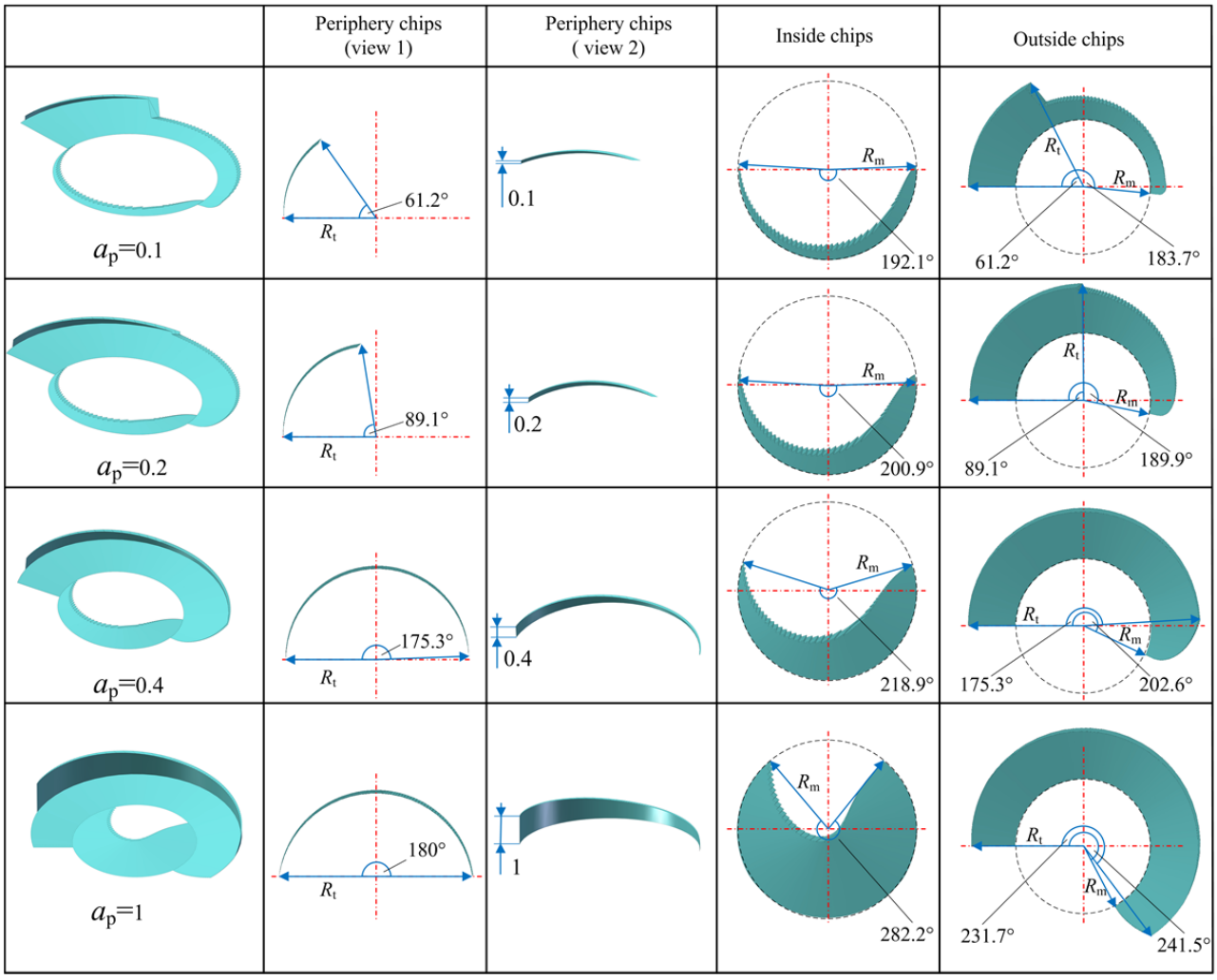

Fig. 32 Variation of undeformed chip geometry under different a_p (e=2)

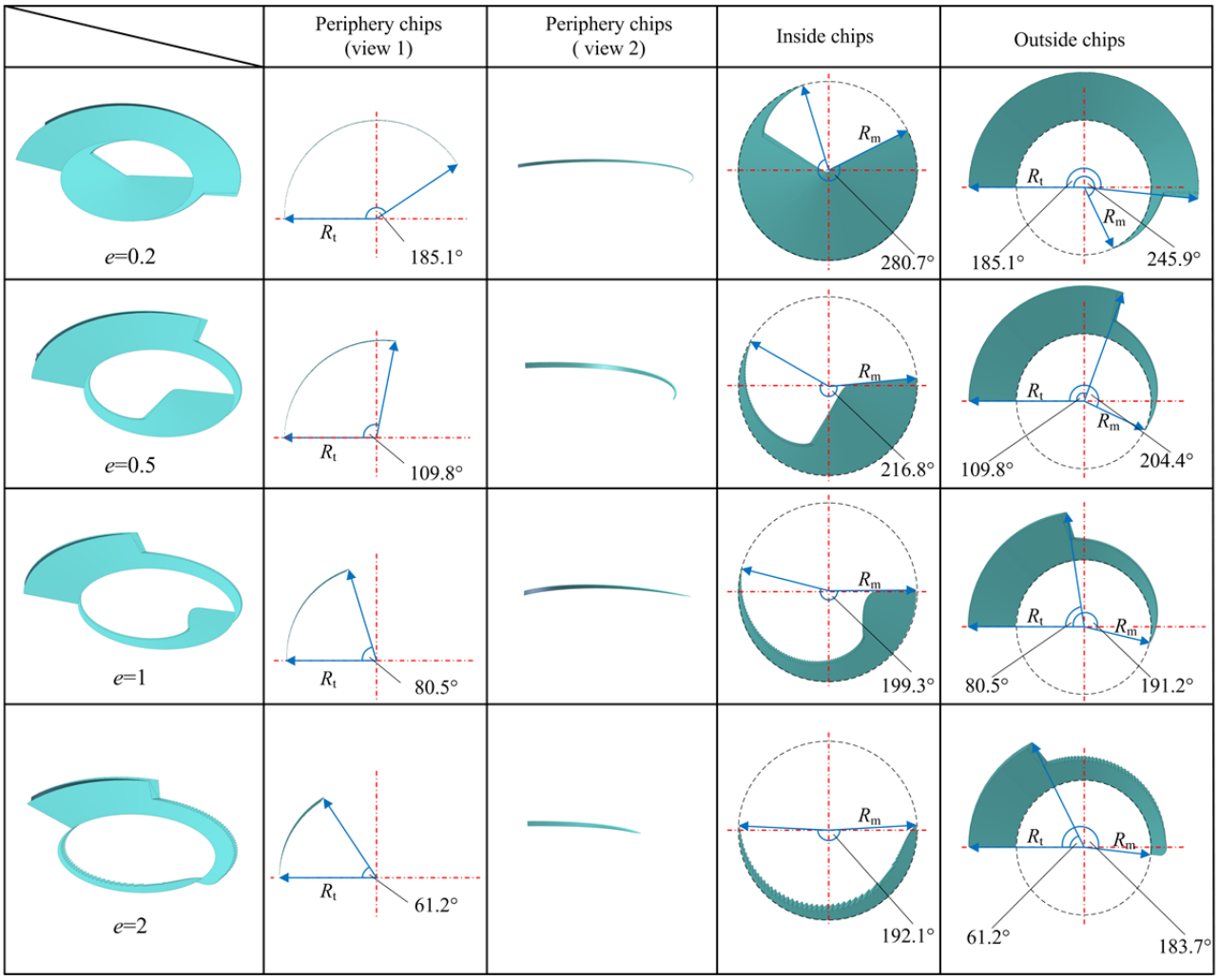

Fig. 33 Variation of undeformed chip geometry under different eccentricity e (a_p=0.1 mm/r)

7 Conclusions

This paper is focused on calculation method of cutting depths (h_{1i} h_{2i} h_{3i}) , cut volumes (V V_1 V_2 V_3) and cut volume ratios (G G_1 G_2 G_3) , description of undeformed chip geometry for helical milling specialized tool. The influence of the depth setting of the helical course (a_p) and eccentricity (e) on cutting depths, cut volume, cut volume ratios was also investigated. Based on the results of calculation and modeling using SolidWorks, the following conclusions can be drawn:

1. The comparison between the structures of the conventional end mill and helical milling specialized tool shows that the specialized tool is more suitable in helical milling process.

2. The calculation methods of cutting depths vary with different cutting parameters (a_p and e). Four types of uncut material morphology may appear and the hole is divided into regions, where the cutting depths change with different rules, to calculate the cutting depths using different methods. The change rate of cutting depths along the radial direction and circumferential direction is

different.

3. The cut volumes (V V_1 V_2 V_3) increase with the increase of a_p and e. When a_p is small, the change rates of the cut volumes are different, the V_1 increases faster than V_1 and V_2, the V_2 increases faster than V_3; the change rates of the cut volumes are the same when a_p beyond some certain value.

4. When e is kept unchanged, the ratios (G G_1) increase with the increase of a_p and reach maximum after a_p beyond some certain value, the ratio G_2 keeps unchanged no matter what the a_p is, the ratio G_3 decreases with the increase of a_p and reaches minimum after a_p beyond some certain value. When a_p is kept unchanged, the ratios (G G_2 G_3) increase with the increase of e, but the ratio G_1 decreases with the increase of e.

5. The changes of a_p and e will affect the unchanged chip geometry and the chip geometry can be optimized by adjusting the value of a_p and e to obtain a good cutting condition.

Acknowledgments

The research is supported by National Natural Science foundation of China (No. 51420105007) and EU H2020 FabSurfWAR (No. 644971).

References

1. Zeilmann RP, Weingaertner WL (2006) Analysis of temperature during drilling of Ti6Al4V with minimal quantity of lubricant. J Mater Process Technol 179:124–127
2. Sharif S, Rahim EA (2007) Performance of coated-and uncoated-carbide tools when drilling titanium alloy-Ti6Al4V. J Mater Process Technol 185:72–76
3. Cantero JL, Tardio MM, Canteli JA, Marcos M, Miguelez MH (2005) Dry drilling of alloy Ti-6Al-4V. Int J Mach Tools Manuf 45:1246–1255
4. Rahim EA, Sharif S (2006) Investigation on tool life and surface integrity when drilling Ti-6Al-4V and Ti -5Al-4V- Mo/Fe. Jap Soc Mech Eng 49:340–345
5. Qin XD, Chen SM, Liu WC, Ni WY, Liu YX (2009) Development and application of hole helical milling technology in aviation manufacturing assembly industry. Aeronautical Manufacturing Technology 6:58–60
6. Lindqvist R, Eriksson I, Wolf M (2001) Orbital drilling of sandwich constructions for space applications. SAE Technical Paper. (No. 2001-01-2571)

7. Sadek A, Meshreki M, Attia MH (2012) Characterization and optimization of orbital drilling of woven carbon fiber reinforced epoxy laminates. CIRP Annals-Manufacturing Technology 61(1), 123–126
8. Tönshoff HK, Friemuth T, Groppe M (2001) High efficient circular milling: a solution for economical machining of bore holes in composite materials. In Proceedings of the Third International Conference on High Speed Machining 287–296, Metz (France)
9. Liu J, Chen G, Ji C, Qin X, Li H, Ren C (2014) An investigation of workpiece temperature variation of helical milling for carbon fiber reinforced plastics (CFRP). Int J Mach Tools Manuf 86:89–103
10. Li Z, Liu Q (2013) Surface topography and roughness in hole-making by helical milling. Int J Adv Manuf Technol 66(9–12):1415–1425
11. Qin XD, Hua S, Ji XL, Liu WC, Chen SM (2010) Research on the surface roughness model for helical milling of die-steel based on response surface methodology. Key Eng Mater 431:346–350
12. Moradi H, Movahhedy MR, Vossoughi G (2012) Dynamics of regenerative chatter and internal resonance in milling process with structural and cutting force nonlinearities. Journal of Sound and Vibration 331:3844–3865
13. Wang, HY, Qin XD, Wang Q (2011) Analysis of cutting forces in helical milling process. In Advanced Materials Research 215: 9–13
14. Wang YF (2014) Research on the helical milling specialized tool for aeronautical hard-machining materials. Master's thesis, Zhejiang University. (in Chinese)
15. Brinksmeier E, Fangmann S, Meyer I (2008) Orbital drilling kinematics. Production engineering 2:277–283
16. Liu G, Wang YF (2014) Research on helical milling specialized tool based on chip-splitting principle. Journal of Mechanical Engineering 50:176–184
17. Denkena B, Boehnke D, Dege JH (2008) Helical milling of CFRP–titanium layer compounds. CIRP J Manuf Sci Technol 1(2):64–69
18. Li Z, Liu Q, Ming X, Wang X, Dong Y (2014) Cutting force prediction and analytical solution of regenerative chatter stability for helical milling operation. Int J Adv Manuf Technol 73:433–442
19. Chen L, Zhang L, Man J (2015) Effect of nominal chip thickness on stability of interrupted

turning. Advances in Mechanical Engineering 7:579178

20. Liu C, Wang G, Dargusch MS (2012) Modeling, simulation and experimental investigation of cutting forces during helical milling operations. Int J Adv Manuf Technol 63:839–850
21. Ventura CE, Hassui A (2013) Modeling of cutting forces in helical milling by analysis of tool contact angle and respective depths of cut. Int J Adv Manuf Technol 68:2311–2319
22. Perez J, Llorente JI, Sanchez JA (2000) Advanced cutting conditions for the milling of aeronautical alloys. Journal of Materials Processing Technology 100(1):1–11